Stabilizing graphene-based organometallic sandwich structures through defect engineering

Pratibha Dev and Thomas L. Reinecke

Stabilizing Graphene-based Organometallic Sandwich Structures through Defect Engineering

Pratibha Dev

NRC post doc residing at Code 6877 Naval Research Laboratory, Washington, D.C. 20375, USA

Thomas L. Reinecke

Naval Research Laboratory, Washington, D.C. 20375, USA

(Dated: January 6, 2015)

In this theoretical work, we propose a chemical route to creating stable benzene-transition metal-graphene sandwich structures. The binding energy of the transition metal to graphene is enhanced through adsorption at appropriate defects, immobilizing the metal onto the graphene web. Capping the metal with a benzene ring further stabilizes the structure. The stability and the magnetic properties of these composite structures vary for different defects such as vacancies and nitrogen substitutionals in graphene. The proposed complexes have high cohesive energies and are either metallic or are small-bandgap semiconductors. Several of the proposed structures also have large spin polarization energies that make them suitable for use as nanomagnets in ambient conditions. This work also sheds light on the experimental results in the field where the sandwich structures may have been successfully created. We show that defect engineering is a viable option for creating designer, graphene-based structures that may play an important role in fields as diverse as spintronics, nanoelectronics, hydrogen storage and catalysis.

In order to develop graphene-based devices, it is desirable to introduce a bandgap in graphene and/or imbue it with additional functionalities, while preserving most of its desirable traits such as its linear energy dispersion, high surface area, and high thermal conductivity [1, 2]. To this end, several different avenues are being explored (see, for example, the review article by Terrone *et al.* [3] and the articles therein), such as creating vacancies, doping graphene with heteroatoms such as nitrogen, or creating more elaborate organometallic complexes [4–7].

Adsorption of transition metals (TMs) is a promising way of doping graphene and modifying its electronic properties without losing the sp^2-bonded structure completely. This ensures high mobilities in the modified graphene unlike, say, in the case of fluorinated graphene that loses its planar structure. Capping the metal atom with a benzene ring or putting another graphene sheet atop this composite structure should further stabilize the structure against the oxidation of the metal atom and improve the binding energy of the structure. Such benzene-transition metal-graphene complexes (from here on written as Bz|M|Gr) have been predicted to form theoretically [4, 5, 8, 9]. However, experimentally, it has proven harder to create such complexes [10]. There is only a single report for these specific complexes [6], although some related structures were recently reported [7, 11]. Some of the difficulties encountered in creating these structures stem from: (a) the high mobility of TMs on graphene, and (b) the high cohesive energies of the TMs [12]. As a result, these metals tend to form clusters [13] making it hard to create TM-dispersed graphene for the sandwich structure.

Several theoretical works [14–17] have explored dispersal of metal atoms on the graphene sheet and the means

with which to control/eliminate clustering of metals. The motives behind these works have varied widely, from the use of the resultant structure for hydrogen storage to its use in spintronics. In our work, we use in-plane defects within graphene in order to overcome the aforementioned challenges in the creation of Bz|M|Gr complexes. The in-plane defects considered here can broadly be categorized as: (a) native defects (monovacancies), and (b) extrinsic impurities. In particular, for the latter we have used nitrogen substituents. Nitrogen undergoes sp^2-hybridization within graphene. Hence, nitrogen can functionalize graphene without affecting its planar structure. Also, nitrogen is versatile in the sense that it can either n- or p-dope the graphene web depending on whether it is incorporated into the structure as graphitic nitrogen, pyridinic nitrogen or pyrrolic nitrogen. Graphitic nitrogen simply replaces a carbon, n-doping the graphene matrix. On the other hand, pyridinic- and pyrrolic nitrogens p-dope the graphene matrix and are present at either the boundaries/edges or next to the carbon vacancies. Although, all of these defects may be present in a nitrogen-doped graphene sample, one can preferentially produce a preponderance of one type of defect over the others [18]. Quite interestingly, we find that the percentage coverage of the metal may play an important role in the structural and magnetic properties of the intermediate metal-graphene (M|Gr) complexes. Once attached to a defect site, the metal can be further immobilized with the help of a benzene ring, creating Bz|M|Gr complexes. As will be shown here, the nature of in-plane defects affects the structural (stability), electronic and magnetic properties of the final graphene-based complexes that are either stabilized or destabilized relative to the pristine (defect-free) Bz|M|Gr. Our results may help to shed

light on the experimental report by Sarkar *et al.* [6] where the sandwich structures may have been created successfully. In the future, a greater understanding of how to use defects to fabricate such designer structures may prove useful in the fields of nano-electronics, spintronics and nano-magnetism.

Calculation Details

The spin-polarized calculations reported here are based on density-functional theory (DFT) within the generalized gradient approximation [19] of Perdew-Burke-Ernzerhof (PBE) [20] to account for the exchange-correlation effects. All calculations are carried out using the Quantum-ESPRESSO package [21]. PBE is known to under-bind the atoms, and so the calculations provide the lower bounds on the binding energies of the composite structures. In order to judge the importance of the local Coulomb interactions in the $3d$ orbitals of the transition metal, we incorporated an effective on-site Coulomb interaction (Hubbard $U{=}3\,\mathrm{eV}$ [22]) for the metal's d states using the DFT$+U$ method [23]. Due to extensive computations required, this was done for only two of the composite structures – metal on pristine graphene and on graphene with an unreconstructed carbon vacancy. It was verified that the DFT and DFT$+U$ results are qualitatively consistent with each other, and so here we present the results within DFT only. These findings are in agreement with those reported by Wehling *et al.* [22].

The work presented here was primarily done with a hexagonal $6 \times 6 \times 1$ (72-atoms) supercell for graphene. In order to study the effects of functional coverage of carbon atoms by the metal, we also used a larger $12 \times 12 \times 1$ (288-atoms) supercell. The smaller supercell corresponds to coverage of about 1.39%, while, the larger structure corresponds to a dilute 0.35% functional coverage. Owing to the expense of such a calculation, only a small, representative subset of the final sandwich structures was created with the 288-atom cell. As we have used the ultrasoft [24] pseudopotentials, we found that a kinetic energy cutoff of $40\,\mathrm{Ry}$ for expanding the wavefunctions and a cut-off of $350\,\mathrm{Ry}$ for charge densities are sufficient. The Monkhorst-Pack scheme [25] was used to generate the Γ-centered, k-point sets equivalent to a $84 \times 84 \times 1$ k-grid for a 2-atom unit cell of graphene. We performed stress-relaxation to obtain the theoretical lattice constant ($a{=}2.466\,\text{Å}$) for the pristine graphene. This lattice constant was then used in all subsequent calculations. In addition, to avoid/reduce any spurious interactions between images, a vacuum layer of about $20\,\text{Å}$-thickness was added in the z-direction.

In Figure 1 we show the in-plane defects that were introduced in the graphene-matrix. With the exception of graphitic nitrogen [Figure 1(c)], the in-plane defects introduce localized defect states [Figures 2(a) and (b)]

derived from the $2p$-states of the carbon and/or nitrogen atoms surrounding the central carbon vacancy. Earlier works have shown that such defect states that originate in $2p$-states of 2nd row elements are well-described within DFT [26–29] and do not require incorporation of additional on-site Coulomb interaction (Hubbard U).

The structures with in-plane defects are used as templates for the metal-graphene (M|Gr) and the final Bz|M|Gr composites. As these calculations are very expensive, we have restricted this study to a few defects and to one transition metal adatom. From among the various TMs, we have chosen to work with chromium to compare the properties of the pristine and modified-Bz|M|Gr sandwich structures with the best-known sandwich compound: bisbenzene chromium molecule, $[\mathrm{Cr}(\eta^6\text{-}\mathrm{C}_6\mathrm{H}_6)_2]$. Here, η stands for hapticity/coordination number of the ligand (benzene) to the metal center (i.e., the number of contiguous ligand atoms bound to the metal). Another consideration for this choice is the cohesive energy of elemental chromium ($\mathrm{E}_C^{expt.}{=}4.10\,\mathrm{eV/atom}$) [12], which is around the average of the cohesive energies for the TMs. In this sense, chromium is a good representative of its class. Our calculated value of cohesive energy for chromium is $3.69\,\mathrm{eV}$. For all structures considered here, the atomic positions are relaxed at each step. The relaxation threshold is set to be equal to or better than $10^{-4}\,\mathrm{Ry/a.u.}$
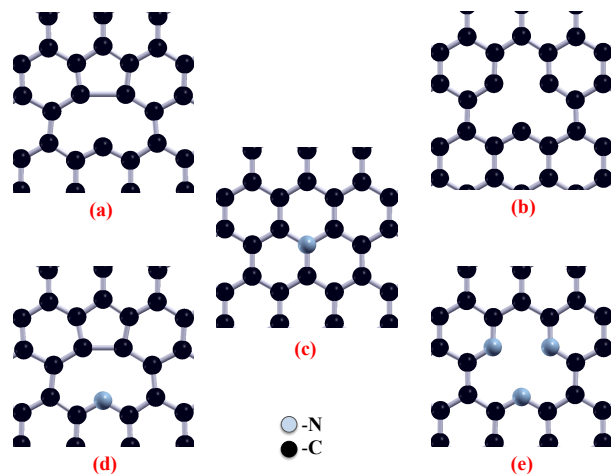

FIG. 1: In-plane defects studied here: (a) Vacancy with Jahn-Teller distortion, $\mathrm{V}_\mathrm{C}^{\mathrm{JT}}$, (b) Symmetric carbon-vacancy, $\mathrm{V}_\mathrm{C}^{\mathrm{Symm.}}$, (c) Graphitic nitrogen (simple substituent), N_C, (d) Vacancy decorated with one pyridinic nitrogen, $1\mathrm{N}_\mathrm{C}\text{-}\mathrm{V}_\mathrm{C}$, and (e) Vacancy decorated with three pyridinic nitrogens, $3\mathrm{N}_\mathrm{C}\text{-}\mathrm{V}_\mathrm{C}$.

Results And Discussion

This section is divided into three subsections. In subsection I, we will briefly discuss our results for the structural, electronic and magnetic properties of several in-

plane defects. In subsection II, we will discuss the modifications of the properties that arise from the addition of metal atom to the pristine and defective graphene. The final subsection III discusses the properties of sandwich-structures that are constructed by capping the metal-atom with benzene. Here, we have used the following notation:

(i) V_C (N_C) stands for carbon vacancy (nitrogen substituent),

(ii) χN_C-V_C stands for nitrogen-vacancy complex (pyridinic defect), where χ is the number of carbons surrounding the vacancy that are substituted by nitrogens,

(iii) Gr:D is written when discussing the graphene sheet containing one of the defects, D, shown in the Figures 1(a)-(e), and

(iv) M|Gr:D (Bz|M|Gr:D) stands for the metal-graphene complex (benzene-metal-graphene complex) with a defect, D, in the graphene lattice.

I. Monovacancies and N-substituents

The carbon monovacancy (V_C) is the simplest native defect that may occur naturally [30] or may be introduced intentionally through irradiation [31–35]. It is a well-studied defect and is known to undergo Jahn Teller (JT) distortion [36]. In the reconstructed structure of Gr:V_C^{JT} [Figure 1(a)], two of the three (initially-equivalent) neighboring carbon-atoms pair-up by coming closer to each other, forming an almost pentagonal ring adjacent to the vacancy. This distortion results in a structure with C_{2v} symmetry that is lower in energy relative to the undistorted structure by about 3.65×10^2 meV. However, recent experimental work by Robertson $et\ al.$ [35] shows that the monovacancies exist in both - lower energy, Jahn Teller reconstructed phase (Gr:V_C^{JT}) as well as the metastable symmetric phase (Gr:$V_C^{Symm.}$). Hence, we have studied not only the reconstructed defect, but also the undistorted symmetric one, Gr:$V_C^{Symm.}$ [Figure 1(b)]. The local structure around the undistorted vacancy has the D_{3h} symmetry.

In the case of graphitic nitrogen [Figure 1(c)], the nitrogen-atom simply substitutes one carbon. Three of its five valence electrons are involved in three σ-bonds with the neighboring carbons, one electron is donated to the π-network, and the last electon n-dopes the graphene web [37]. We have also studied two pyridinic defects: $1N_C$-V_C that results in a structure with the C_{2v} symmetry [Figure 1(d)], and the $3N_C$-V_C-defect (D_{3h} symmetry) as shown in Figure 1(e). In the case of a pyridinic defect, the incorporated nitrogen undergoes sp^2 hybridization and replaces a carbon atom that is the nearest
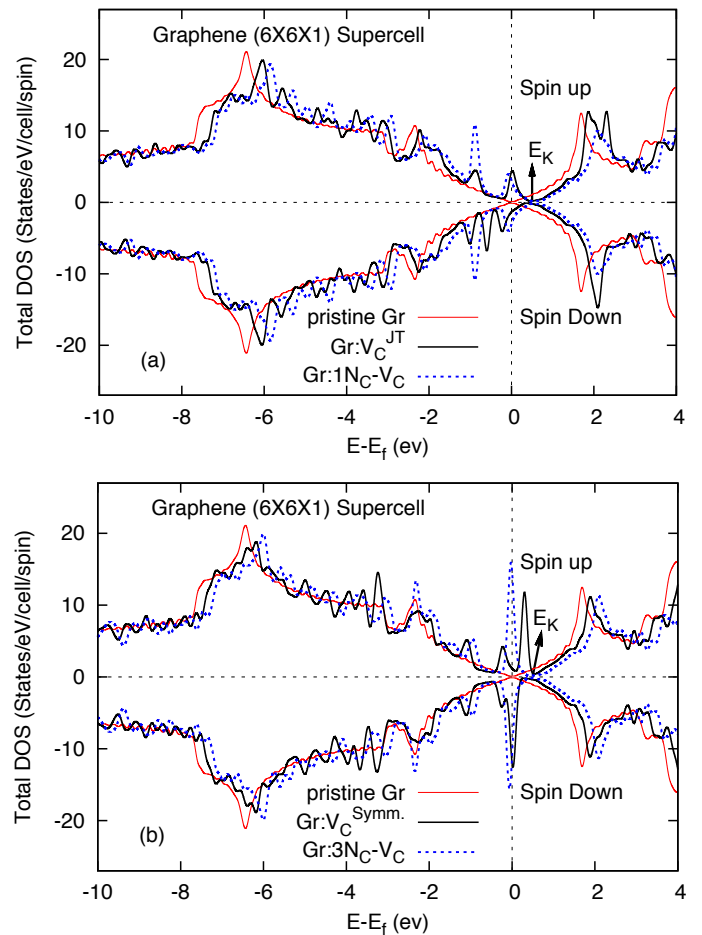

FIG. 2: (a) Total DOS for pristine graphene and the acceptor-like defects with (a) the C_{2v} symmetry – V_C^{JT} and $1N_C$-V_C, and (b) the D_{3h} symmetry – $V_C^{Symm.}$ and $3N_C$-V_C. The Dirac point for the defective structures is located approximately at E_K Here, E_f is the Fermi energy.

neighbor to a carbon vacancy. Two of the sp^2-hybridized orbitals of the pyridinic nitrogen form σ-bonds with the neighboring carbons, the third sp^2-hybridized orbital contains the lone-pair that plays an important role in the chemistry of the defect, and the last electron is donated to the π-network.

In Table I, we list several properties of the in-plane defects in graphene for the $6 \times 6 \times 1$ supercell. The presence of the monovacancy and pyridinic nitrogen results in the hole-doping of graphene. This is evident from the increase in its work function (ϕ) when compared to the case of pristine graphene. Here, the work function is calculated as the energy difference between the Fermi energy and the electrostatic potential in the vacuum region (far from the surface). As expected, the simple substitutional nitrogen electron-dopes graphene. The values for work function reported here are consistent with those obtained earlier by others (for example, see Schiros $et\ al.$ [37]), with the differences attributable to the choice

System	ϕ (eV)	Doping Type	$m^{6\times6\times1}$ (μ_B)	$\Delta E^{Pol.}$ (meV)
$Gr^{Pristine}$	4.24	undoped	0.00	N.M.
$Gr:V_C^{JT}$	4.56	p-doped	1.58	370.0
$Gr:V_C^{Symm.}$	4.46	p-doped	0.22	136.7
$Gr:N_C$	3.70	n-doped	0.00	N.M.
$Gr:1N_C-V_C$	4.72	p-doped	0.00	N.M.
$Gr:3N_C-V_C$	4.69	p-doped	0.08	5.0

TABLE I: Work functions (ϕ), doping-type, net magnetic moments ($m^{6\times6\times1}$) and spin polarization energies, $\Delta E^{Pol.}$ (=difference in total energies of spin-unpolarized and spin-polarized states) for the graphene sheet without and with in-plane defects ($6 \times 6 \times 1$ supercells). N.M. in the last column means that the structure is non-magnetic.

of the exchange-correlation functional employed in the calculations. The hole-doping of graphene is also evident in Figures 2(a) and (b), where the zero of the energy is at the Fermi energies of the respective structures and E_K gives the approximate location of the Dirac-point in the p-doped structures. Only in the case of pristine graphene do these two energies coincide.

Table I also lists the magnetic properties of several defects in graphene. The spin polarization energy, $\Delta E^{Pol.}$ is defined as the energy difference between the spin unpolarized and spin-polarized structures. The magnetic properties of the carbon vacancies and nitrogen substituents are described in previous works [38, 39] and for the sake of brevity, will not be discussed here in any detail.

The structural and magnetic properties of the larger 288-atom supercells are found to be similar to those for the smaller cells, with the exception of the $Gr:3N_C-V_C$. In the case of this pyridinic defect, the magnetic properties show a dependence on the defect density, with the larger structure being non-magnetic. An earlier work by Kattel et. al [39] reported the $Gr:3N_C-V_C$-structure to be magnetic, with a small magnetic moment of $0.46\,\mu_B$. A much smaller $4\times4\times1$ supercell (32 atoms) was used in their calculation and hence, they were considering very high defect density. Kattel et. al attributed the small magnetic moment ($0.46\,\mu_B$) in their structure to the direct overlap between the nitrogen wave functions. In order to explore this matter further, we also performed the calculation with a smaller $4 \times 4 \times 1$ supercell containing this defect, and found a magnetic moment of $0.58\,\mu_B$ and a polarization energy of $11.6\,meV$, consistent with the earlier results [39]. The sensitivity of the magnetic properties of this structure to the density of the pyridinic-defect may be attributed to: (i) the overlap of defect states in the case of larger defect density, and (ii) the presence of a very-localized DOS (see Figure 2) at the Fermi level, arising from the lone pairs on the three nitrogen atoms. The presence of such states

indicates system instabilty vis-à-vis material properties such as magnetism (Stoner criterion).

II. M|Gr Compostite Structures

The next step in this work was the creation of metal-graphene complexes formed by adsorption of metal onto graphene, both with and without defects. For the sake of comparison, we also carried out these calculations for a fictitious system consisting of chromium adsorbed onto a single benzene ring. Tables II and III summarize the structural, electronic and magnetic properties of the metal-graphene complexes. In Table II, the binding energy of the chromium-graphene complex is defined as the difference in the total energies of the reactants considered separately and the product (M|Gr):

$$\Delta E_{M|Gr}^{BE} = E_{Cr} + E_{Gr} - E_{M|Gr} \qquad (1)$$

System	$\Delta E_{M|Gr}^{BE}$ (eV)	$BL_{M-Gr}^{av.}$ ($h_z^{av.}$) (Å)	$\theta_{av.}$	$R.D._{\theta}$
$M|Gr^{Pristine}$	0.12	2.57 (2.13)	90.00°	0.00
$M|Gr:V_C^{JT}$	5.80	1.86 (1.04)	100.56°	0.54
$M|Gr:V_C^{Symm.}$	6.17	1.86 (1.04)	100.57°	0.54
$M|Gr:N_C$	-			
$M|Gr:1N_C-V_C$	4.65	1.87 (1.04)	99.99°	0.51
$M|Gr:3N_C-V_C$ (Metastable)	3.56	1.96 (1.19)	97.08°	0.36
$M|Gr:3N_C-V_C$ (Ground State)	3.57	1.81 (0.89)	101.35°	0.58
M|Bz	0.10	2.67 (2.27)	90.00°	0.00

TABLE II: Structural properties of the complexes of metal on benzene/graphene sheet (for the $6 \times 6 \times 1$ supercell). Here, $\Delta E_{M|Gr}^{BE}$ is the binding energy, $h_z^{av.}$ is the average height of the metal relative to the carbon or nitrogen atoms, $BL_{M-Gr}^{av.}$ is the average bond length between the metal and atoms on graphene, and the measure, $R.D._{\theta} = (\theta_{av.} - 90°)/(109.47° - 90°)$ gives the departure from the sp^2 structure at the site of complex-formation.

As can be seen in Table II, the chromium atom is barely bound to the pristine graphene ($M|Gr^{Pristine}$) or to the benzene (M|Bz). There is a very small (ionic) charge transfer of $0.15\,e$ from the metal atom to the graphene surface (see Table III). This changes considerably upon the introduction of defects in graphene. Here, we have studied defects that either p-dope or n-dope graphene. Depending on their nature, we observe two different behaviors:

(i) The carbon vacancies and pyridinic-nitrogen p-dope graphene and introduce acceptor-like states

in graphene. The latter helps in the binding of metal to the graphene web by increasing the reactivity at the defect site, while the p-doping of graphene helps the binding by increasing the electrostatic attraction between the oppositely-charged donor (Cr) and the acceptor (defective-graphene). The binding between chromium and these defects in graphene shows an admixture of ionic and covalent behavior. There is a strong hybridization between the nitrogen/carbon $2p$-derived defect states and primarily, the $3d$-states of the metal atom. The p-type doping [15, 16] of graphene due to these defects also increases the charge (Δq_{Cr}) that is transferred from the metal to graphene (see Table III).

(ii) Unlike the carbon vacancies and pyridinic-nitrogen, the graphitic nitrogen (N_C) n-dopes graphene and introduces donor-like states. The presence of the donor-like graphitic nitrogen has an adverse effect on the binding of the metal to graphene. We found that the interaction between the metal and the n-doped graphene was possibly repulsive. The resultant structures for $M|Gr:N_C$ could not be relaxed into a bound state for the two adsorption sites (for the metal) that were explored in this work.

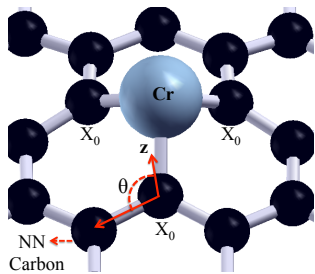
FIG. 3: Introduction of sp^3-character in defective graphene ($V_C^{Symm.}$) upon adsorption of chromium.

In order to create the final sandwich complexes, it is important to be able to create the intermediate $M|Gr$ structures with well dispersed metal atoms. As discussed above, these intermediate structures do not form in the presence of n-type defects such as the graphitic nitrogen and hence, we will not consider such defects in any detail here. On the other hand, the acceptor-like defects aid in binding chromium to the surface. The differences in the strengths of binding of the metal-atom to pristine graphene and to the acceptor-like defect sites should mean that the defect sites will act as sink for the metal atoms that will migrate from the defect-free regions of graphene until they bind at the defect. In addition, the binding energy of the metal at the defect in graphene exceeds the cohesive energy of elemental chromium (3.69 eV) for almost all of the acceptor-type defects (see Table II). Therefore, these defects may be used for dispersal of the metal onto the graphene sheet.

The only exception is the pyridinic defect, $Gr:3N_C$-V_C, where the binding energy of the metal atom to graphene (3.57 eV) is comparable to cohesive energy of chromium atoms to each other (3.69 eV). As the two energies are comparable, the kinetics might be the determining factor between the effective metal dispersal on graphene and the clustering of TM-atoms to form aggregates on the graphene surface.

For the acceptor-type defects in graphene, the metal binds in a tridentate fashion, forming very strong bonds with the carbon/nitrogen atoms that surround the vacancy. This introduces sp^3-character in the graphene web, resulting in a local puckering of the graphene sheet as the atoms in graphene's plane (called X_0's in Figure 3, where X=N, C) bond to the chromium atom and are raised above the plane of graphene. One can quantify the degree of this local sp^3 character by the average value, $\theta_{av.}$, of the angles formed between the z-axis (axis perpendicular to the plane of graphene) and the new σ-orbitals formed upon rehybridization of X_0's and the carbon atoms that are their nearest neighbors [Figure 3]. Another useful measure of the local sp^3 character is the (normalized) relative difference between the angle $\theta_{av.}$ and the angle in case of an ideal sp^2 structure ($90°$): R.D.$_\theta = (\theta_{av.} - 90°)/(109.47° - 90°)$. R.D.$_\theta$ takes values between [0, 1] for the interval $\theta = [90°, 109.47°]$ [40]. The endpoints of the interval correspond to pure sp^2 and pure sp^3 hybridizations. These structural properties are listed in Table II.

It is also interesting to note that the binding energies listed in Table II do not follow obvious trends in going from one defect to another. For example, the metal atom binds less strongly with graphene that contains reconstructed vacancy [$Gr:V_C^{JT}$] as compared to graphene containing the unreconstructed carbon vacancy [$Gr:V_C^{Symm.}$]. This can be understood as a result of several factors that affect the stability of the composite structure. The metal atom is considerably larger than the carbon atoms and it tends to sit above the graphene plane and in the middle of the hollow region left by the vacancy. A symmetrical placement relative to the carbon atoms in the graphene plane maximizes the carbon-metal bonds, resulting in a stable structure. Thus, the metal adatom tends to stabilize the unreconstructed, symmetric $V_C^{Symm.}$ [D_{3h} symmetry]. This can be seen even when one starts from a vacancy that has undergone JT distortion, V_C^{JT}. Upon adsorption of the metal onto the structure, the system undergoes a near-complete reversal in its structural modifications that were incurred during JT distortion. As the metal forms bonds with the three carbon atoms surrounding the vacancy, it breaks the weak bond that had formed between two of these carbons [41]. The final structure almost attains the geometry of unreconstructed $V_C^{Symm.}$ with some of the strain still present in the structure. The two factors – preference for the higher symmetry of the unreconstructed carbon vacancy, $V_C^{Symm.}$, and

a greater strain in graphene with V_C^{JT} – result in better binding of chromium to the former. Similar stabilization of the symmetric defect upon addition of metal adatom was also observed by the others (e.g. Santos *et al.* [42]).

M|Gr:$3N_C$-V_C shows very interesting structural and magnetic properties. The structure has not only a ground state but also a metastable state that is higher in energy than the former configuration by about 11.0 meV. The ground state shows a greater covalent-character than the metastable state of the structure. This can be seen in the lower height of the metal above graphene and the greater strength of interaction, as well as in the greater distortion of the graphene sheet for the ground state structure (Table II) as compared to its metastable configuration. In addition, in the metastable structure, with increased ionicity, there is a greater transfer of charge from the metal into graphene (Table III). These electronic and structural properties have a large effect on the magnetic properties of the two structures.

System	$m_{M|Gr}$ (μ_B)	m_{Cr} (μ_B)	$\Delta E^{Pol.}$ (eV)	Δq_{Cr} (e)
M|Gr^{Pristine}	5.61	5.39	1.90	0.15
M|Gr:V_C^{JT}	2.00	2.47	0.97	0.38
M|Gr:$V_C^{Symm.}$	2.00	2.47	0.97	0.38
M|Gr:N_C	-			
M|Gr:$1N_C$-V_C	2.99	3.01	1.10	0.39
M|Gr:$3N_C$-V_C (Metastable)	4.34 (HS)	3.92	0.57	0.47
M|Gr:$3N_C$-V_C (Ground State)	1.20 (LS)	2.21	0.58	0.44

TABLE III: Net magnetic moments ($m_{M|Gr}$) of the complexes ($6 \times 6 \times 1$ supercell), along with the metal's contributions to the net moment (m_{Cr}). Here, Δq_{Cr} is the charge transferred from chromium onto graphene. LS and HS stand for the low spin and the high spin state, respectively.

Table III gives the net magnetic moments and polarization energies of the metal-graphene complexes for the $6 \times 6 \times 1$ supercell. Owing to a very small interaction between chromium atom and pristine graphene, the net magnetic moment of the composite structure, M|Gr^{Pristine}, is close to the atomic magnetic moment. In this case, the interaction is mostly ionic, with some charge being transferred ($\sim$0.15 electrons) from the chromium $4s$ into the graphene web. This can be seen from the DOS and the projected DOS in Figure 4(a). The Dirac point is visible in the minority-spin channel, albeit shifted to about 0.39 eV below Fermi energy due to n-doping. The chromium $3d$ and $4s$-derived states in the M|Gr^{Pristine} composite are strongly localized on the metal and are atomic in nature.

In case of the simple vacancies (with or without JT distortion in the starting structure), the composite structure
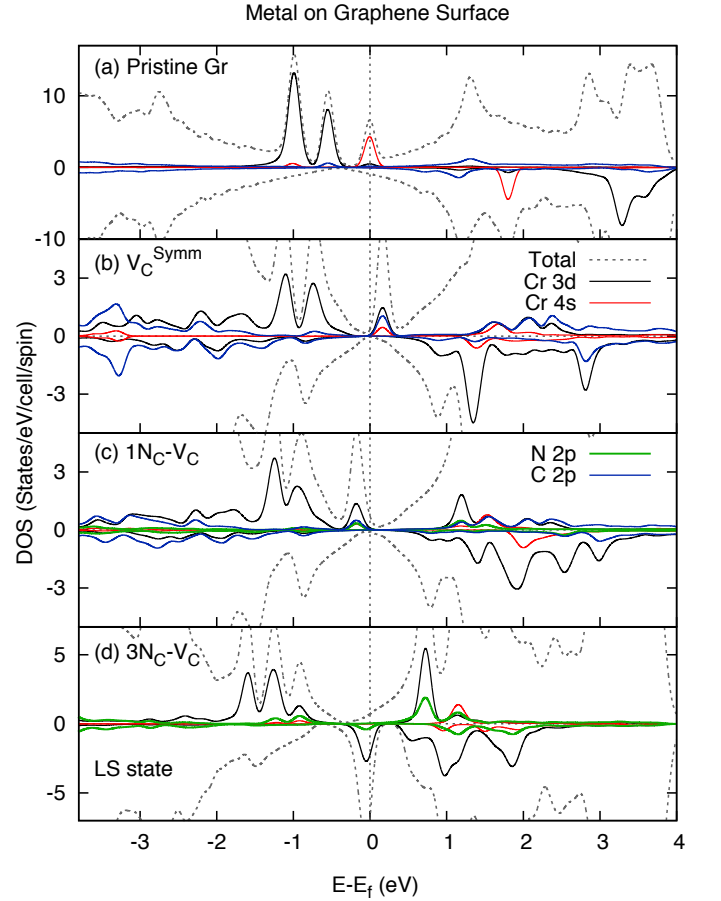

FIG. 4: Total and projected DOS plots of some of the chromium-graphene complexes. Along with DOS projected onto the chromium 3d and 4s, we have included the PDOS of the nearest neighbor atoms (carbon/nitrogen) on the graphene surface. Majority spin is plotted along the positive ordinate and minority spin along the negative ordinate in each subplot.

[M|Gr:V_C] is non-metallic and has a small band gap of 1.06×10^2 meV. It also shows a net magnetic moment of exactly 2.00 μ_B. This can be understood within the molecular orbital theory to be a result of the hybridization of the $3d$-states of the chromium atom with the defect levels of the carbon vacancy [42]. This hybridization can be seen in the overlap in DOS of carbon's 2p-derived and the chromium's $3d$ and $4s$-derived states [see Figure 4(b)]. This picture can be extended to M|Gr : $1N_C$-V_C (symmetry of the composite: C_S), where the high spin configuration results in a net magnetic moment of about 2.99 μ_B.

The complex of the metal on the pyridinic defect, $3N_C$-V_C, shows very interesting electronic and magnetic behavior. The complex has both localized electrons (in the minority spin-channel) and delocalized conduction electrons in the majority-spin channel [Figure 4(d)] around the Fermi energy. The ground state of M|Gr : $3N_C$-V_C

has a low-spin (LS) configuration with a net magnetic moment of $1.20\,\mu_B$. On the other hand, the metastable structure with a greater ionic-character had a high-spin (HS) configuration (m=4.34 μ_B). These results can be understood within the molecular orbital theory [43]. In the M|Gr : $3N_C$-V_C composite, the local structure has C_{3v} symmetry. Within this symmetry, the chromium $3d$-states split into two doublets - $d_{yz,zx}$ and $d_{x^2-y^2,xy}$ belonging to the E-representation and a singlet d_{z^2} belonging to the A_1 representation (Figure 5). In the ground state configuration, a strong hybridization between the Cr $3d$ and the defect states (nitrogen-$2p$ derived) results in a large separation between the resulting bonding and anti bonding hybrid states in the majority-spin channel [see, Figure 5(a)]. The antibonding majority-spin states are unoccupied, while the bonding hybrid states in the minority spin channel (belonging to the E-representation) become partially occupied [Figure 5(a)], leading to a LS-configuration [Figure 5(a)]. This is also reflected in the Löwdin charge analysis that shows a partial filling of chromium's $3d$ states in the minority spin channel: $d^{3.43\uparrow}d^{1.37\downarrow}$. On the other hand, there is a weaker hybridization between the Cr $3d$ and the nitrogen-$2p$ derived defect states in the metastable HS-configuration. As a result, the separation between the bonding and antibonding hybrid states in the majority spin channel is smaller when compared to the ground state. These bonding as well as antibonding majority spin states are filled first, while the minority spin states with $3d$-character mostly lie above the Fermi level in this case [Figure 5(b)]. The resultant electronic configuration in the HS state (Löwdin charge analysis) is: Cr $d^{4.21\uparrow}d^{0.52\downarrow}$.
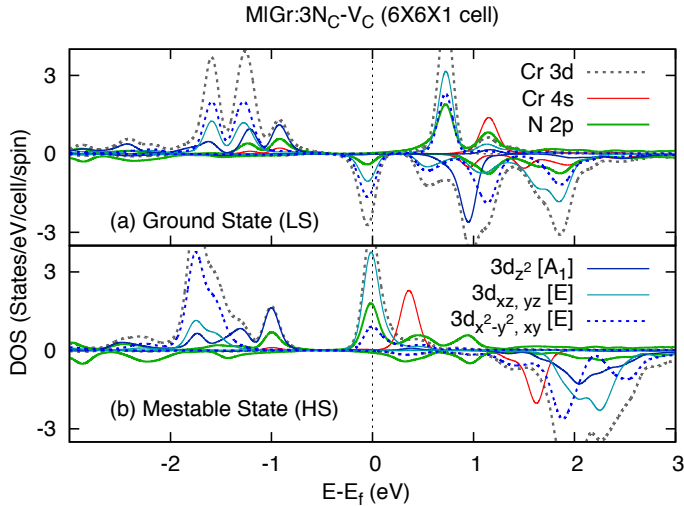

FIG. 5: DOS projected onto the chromium's 3d and 4s as well as onto the nitrogen atoms for (a) the ground state (LS), and (b) the metastable state (HS) of the M|Gr:$3N_C$-V_C structure. Majority spin is plotted along the positive ordinate and minority spin along the negative ordinate in each subplot.

We also carried out a small subset of these calculations for the $12 \times 12 \times 1$ supercells. In order to reduce the computational cost, we chose the structures with higher symmetries: pristine graphene, $V_C^{Symm.}$ and $3N_C$-V_C. In the first two cases, we found that the structural, electronic and magnetic properties of the larger composite structures did not change qualitatively compared to those in the smaller supercell. On the other hand, the pyridinic defect, $3N_C$-V_C, showed a strong dependence on the functional coverage.

The ground state of the M|Gr : $3N_C$-V_C composite changes from the LS configuration for the 72-atom supercell to a HS configuration for the 288-atom supercell. As mentioned earlier, the binding of the metal at the defect site on the surface is partially covalent as indicated by the binding strength as well as the binding height. It is also partially ionic as indicated by the transfer of charge between the components of the composite. The binding height and hence, the extent of hybridization of metal states with those of graphene results from the interplay of:

(i) the electrostatic attraction between the oppositely-charged donor (Cr) and the acceptor (defective-graphene) [14],

(ii) the onsite-Coulomb repulsion upon pairing of electrons in the LS state, and

(iii) the energy cost of the strain resulting from the co-existence of the sp^2 and sp^3-bonded carbons within the graphene lattice [44].

In the limit of dilute functional coverage (as in the 288-atom supercell), there is a low concentration of sp^3-bonds formed between the metal and the locally puckered graphene sheet. This energy cost due to the strain within the mostly sp^2-bonded lattice increases with the functional coverage until a concentration is reached where there are more sp^3-bonded carbons than the sp^2-bonded ones. In this case, the latter become responsible for the strain in the structure (as in the 72-atoms supercell). The strain is then minimized if there is an increased covalency within the structure, resulting in a mostly sp^3-bonded structure. Thus, the low spin state becomes the ground-state in the 72-atom supercell. On the other hand, in the limit of dilute concentration, as in the 288-atom supercell, the strain energy is minimized by the increased ionic-character of the bonding between the metal and the defect. This results in a HS ground state that also minimizes its energy by avoiding the cost of pairing of electrons in the states derived mostly from the metal's $3d$ states.

Thus, depending on the nature of the defects, one may be able to use the functional coverage to control the electronic and hence the magnetic properties of metal-dispersed graphene. In dilute limits, the defect-stabilized

M|Gr system will have a mostly sp^2-bonded lattice away from the site of complex formation and hence, may retain one of the desirable features of graphene - its high mobility. It should also be pointed out that different defects produce metal-graphene networks with different properties. For example, the V_C-defect results in a structure with vanishing DOS at the Fermi level, while the composite structures containing pyridinic-nitrogen defects have both localized as well as delocalized states at the Fermi level. These structures may prove to be of interest for applications such as spin-valves without a further need to modify their properties. Depending on the application, it may also be desirable to stabilize these structures further by the addition of a benzene-molecule to cap the metal. In addition to providing stability, the benzene ring can also be used as a local gate through the addition of electron-donating or electron-withdrawing substituents in benzene [5].
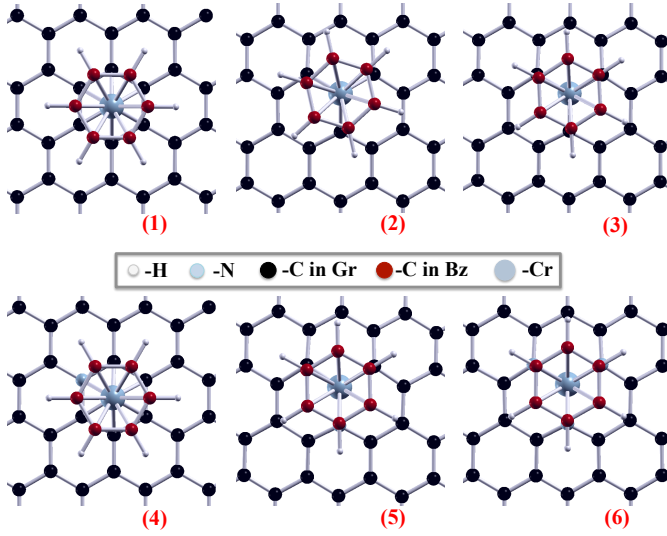
III. Bz|M|Gr **Compostite Structures**

FIG. 6: The staggered, eclipsed and distorted-eclipsed geometries at equilibrium formed by the Bz|M|Gr complexes created using different graphene templates: (1) pristine graphene (2) V_C^{JT}, (3) $V_C^{Symm.}$, (4) N_C, (5) $1N_C$-V_C, and (6) $3N_C$-V_C.

Bz|M|Gr complexes show several distinct structures (see Figure 6) that result in different bonding properties–bond lengths and bond strengths–amongst the systems considered here. Table IV lists the structural properties of the complexes using a $6 \times 6 \times 1$ supercell. The corresponding values of binding energies and bond lengths for the molecule, bisbenzene chromium, are also provided for the sake of completeness. The capping of |M|Gr-complex with a benzene ring stabilizes the system. To elucidate the role played by benzene in the stabilization

of the structures, Table IV lists two binding energies: $\Delta E_{Bz|M|Gr}^{BE}$ and $\Delta E_{Bz|M|Gr}^{'BE}$. The former is the binding energy of the entire complex, defined as:

$$\Delta E_{Bz|M|Gr}^{BE} = [E_M + E_{Gr} + E_{Bz}] - E_{Bz|M|Gr} \qquad (2)$$

The related quantity, $\Delta E_{Bz|M|Gr}^{'BE}$, is defined as the energy stabilization in the final structure by adding benzene to the |M|Gr structures:

$$\Delta E_{Bz|M|Gr}^{'BE} = [E_{M|Gr} + E_{Bz}] - E_{Bz|M|Gr} \qquad (3)$$

As discussed in the previous section, the acceptor-like defects act as the binding sites for the adsorption of the metal adatom. Thus, the subsequent formation of benzene-chromium-graphene sandwich structures will preferentially occur at these defect sites. As compared to Bz|M|Gr^{Pristine}, all complexes with acceptor-like defects show large increases in stability. A comparison of the binding energies, $\Delta E_{Bz|M|Gr}^{BE}$ in Table IV and $\Delta E_{M|Gr}^{BE}$ in Table II, shows that a very large fraction of the binding energy of such a sandwich structure comes from the bonding of chromium to the defect.

The $\Delta E_{Bz|M|Gr}^{'BE}$-values are also instructive in understanding the energy stabilization upon the addition of benzene to |M|Gr-structure. These binding energies are among the highest for the complexes formed on pristine graphene and at the $3N_C$-V_C-defect. Both of these sandwich structures satisfy Langmuir's 18-electron rule [45, 46] for transition metal complexes, which is also used to explain the stability of the $Cr(\eta^6\text{-}C_6H_6)_2$ molecule. In the latter, 6π-electrons from each benzene mix with the 6-electrons from the chromium atom to form a 18-electron closed-shell configuration. In case of the Bz|M|Gr : $3N_C$-V_C complex, the closed shell configuration is reached by the 6-electrons in the three lone-pairs on the nitrogens, 6π-electrons from the benzene and the 6-electrons from the chromium atom.

Figure 7 shows the effects of benzene on the DOS of the complexes. In all of the Bz|M|Gr-structures studied here, benzene's contribution to the total DOS around the Fermi energy is very small. Nonetheless, by hybridizing with the metal's d-states, benzene changes the electronic structure of the complex, reducing the splitting between majority and minority spin bands relative to the respective M|Gr structures. This changes the electronic and hence, magnetic properties of the pristine and the defect-stabilized sandwich complexes relative to their M|Gr counterparts in following ways:

(i) The Bz|M|Gr^{Pristine}-complex is a metallic structure [Figure 7(a)], with a small net magnetic moment of $0.37\,\mu_B$ (Table V). In contrast, the $Cr(\eta^6\text{-}C_6H_6)_2$ molecule is a non-magnetic structure where

| System | $\Delta E^{BE}_{Bz|M|Gr}$ | $\Delta E'^{BE}_{Bz|M|Gr}$ | $BL^{av.}_{M-Gr}$ ($h^{av.}_z$) | $BL^{av.}_{Bz-M}$ ($h^{av.}_z$) | $\theta_{av.}$ | $R.D._\theta$ |
(6 × 6 × 1 cell)	(eV)	(eV)	(Å)	(Å)		
$Bz|M|Gr^{Pristine}$	1.94	1.81	2.22 (1.69)	2.14 (1.59)	90.04°	0.00
$Bz|M|Gr : V_C^{JT}$	6.75	0.95	1.89 (1.11)	2.48 (2.04)	101.46°	0.59
$Bz|M|Gr : V_C^{Symm.}$	7.12	0.96	1.89 (1.11)	2.48 (2.04)	101.48°	0.59
$Bz|M|Gr : N_C$	1.53	-	2.20 (1.68)	2.15 (1.61)	90.25°	0.01
$Bz|M|Gr : 1N_C\text{-}V_C$	5.47	0.83	1.93 (1.16)	2.44 (1.99)	100.51°	0.54
$Bz|M|Gr : 3N_C\text{-}V_C$	5.51	1.94	1.98 (1.24)	2.19(1.67)	100.43°	0.54
$Cr(\eta^6\text{-}C_6H_6)_2$	2.95	2.85	-	2.14(1.60)	90.00°	0.00

TABLE IV: Structural properties of the Bz|M|Gr complexes. $\Delta E^{BE}_{Bz|M|Gr}$ is the binding energy of the complex and $\Delta E'^{BE}_{Bz|M|Gr}$ is the energy stabilization upon addition of benzene to the |M|Gr structure. $BL^{av.}_{M-Gr}$ is the average bond length between chromium and the nearest neighbor atoms in graphene, and $BL^{av.}_{Bz-M}$ is the average distance between chromium and benzene.

the metal atom, encased symmetrically by benzene-rings on the two sides, maintains its formal zero-oxidation state (see Δq_{Cr} in Table V).

(ii) As can be seen in Figure 7(b), the capping of the $M|Gr : V_C$ structure with the benzene ring does not destroy the band gap. The resultant structure, $Bz|M|Gr : V_C$, shows a small band gap of about 0.92×10^2 meV. The structure has a magnetic moment of exactly $2.00\,\mu_B$, albeit with a reduced polarization energy (Table V) relative to the $M|Gr : V_C$ structure (Table III).

(iii) The two pyridinic defects are metallic structures [Figure 7(c)-(d)]. The rearrangement of the states around the Fermi energy reduces the polarization energies (Table V) of the complex relative to the benzene-free structures (Table III). As a result, these structures also have smaller magnetic moments relative to their M|Gr counterparts.

| System | $m_{Bz|M|Gr}$ | m_{Cr} | $\Delta E^{Pol.}$ | Δq_{Cr} |
	(μ_B)	(μ_B)	(eV)	(e)
$Bz|M|Gr^{Pristine}$	0.37	0.43	0.03	0.08
$Bz|M|Gr : V_C^{JT}$	2.00	2.23	0.68	0.23
$Bz|M|Gr : V_C^{Symm.}$	2.00	2.23	0.73	0.23
$Bz|M|Gr : N_C$	0.00	0.00	0.00	0.00
$Bz|M|Gr : 1N_C\text{-}V_C$	2.98	2.66	0.37	0.29
$Bz|M|Gr : 3N_C\text{-}V_C$	1.13	1.61	0.39	0.22
$Cr(\eta^6\text{-}C_6H_6)_2$	0.00	0.00	0.00	0.03

TABLE V: Net magnetic moments ($m_{Bz|M|Gr}$) of the sandwich complexes (6 × 6 × 1 supercell), along with the metal's contributions to the net moment (m_{Cr}). The polarization energy, $\Delta E^{Pol.}$ and the charge transferred from chromium onto graphene, Δq_{Cr}, show a departure from the properties of the molecular analogue $Cr(\eta^6\text{-}C_6H_6)_2$, except in the case of $Bz|M|Gr : N_C$.

We find that the structural and electronic properties for the larger $12 \times 12 \times 1$ supercell do not change appreciably. For example, the local values of the $\theta_{av.}$ are 90.02°, 101.39°and 100.62° for the $Bz|M|Gr^{Pristine}$, $Bz|M|Gr : V_C^{Symm.}$, and $Bz|M|Gr : 3N_C\text{-}V_C$, respectively. These are comparable to the $\theta_{av.}$ values calculated for the corresponding $6 \times 6 \times 1$ supercells (see Table IV). Likewise, the magnetic properties of these complexes calculated for the larger supercells are comparable to those given in Table V. The magnetic moments (polarization energies) of the larger structures are found to be $0.52\,\mu_B$ $(0.07\,\text{eV})$, $2.00\,\mu_B$ $(0.79\,\text{eV})$ and $1.08\,\mu_B$ $(0.39\,\text{eV})$ for the sandwich structures formed on $Gr^{Pristine}$, $Gr : V_C^{Symm.}$, and $Gr : 3N_C\text{-}V_C$, respectively. Hence, we find that for both of the functional coverages considered here, the defect-stabilized sandwich structures have high polarization energies ($\geq 0.37\,\text{eV}$), suggesting that the spin-polarized state should survive well above room temperature. This should make them suitable for use as nanomagnets in ambient conditions.

In addition, our study of sandwich structures revealed that the sp^2-hybridization of graphene remains intact only in the case of sandwich structures formed on pristine graphene and in case of graphene with graphitic nitrogen (see $\theta_{av.}$ in Table IV). However, the sandwich structures are more likely to form at the acceptor-type defects. In all of these defect-stabilized systems, there is an emergence of sp^3-character within graphene upon formation of the sandwich structure. This is found to be the case for all functional coverages considered in this work. The two features: (i) a greater propensity to form composites at appropriate defect sites, and (ii) the appearance of sp^3-character within the graphene matrix upon formation of the composite structures, should occur concurrently. The latter effect would be missing if the sandwich structures were formed with the pristine graphene. Experimentally, this would appear as a substantial increase in the intensity of D-band in the Raman spectra, as well as a decrease in the mobility compared to pristine graphene. In
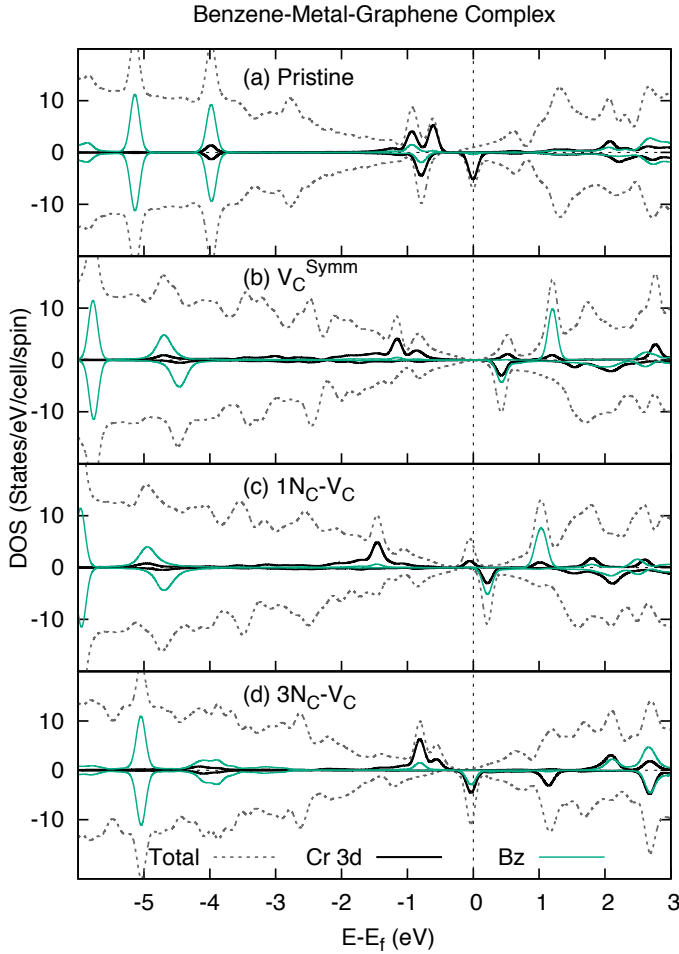
Benzene-Metal-Graphene Complex

FIG. 7: Total and projected DOS plots of various Bz|M|Gr complexes. The DOS projected onto the chromium 3d and onto the benzene molecule (Bz) are included here. Majority spin is plotted along the positive ordinate and minority spin along the negative ordinate in each subplot.

fact, a large increase in D-band intensity was indeed observed experimentally [6] upon formation of the Bz|M|Gr complexes, possibly indicating complex-formation at the defect sites. Sarkar *et al.* [6, 7] also reported a decrease in conductance upon complex formation for a related structure, Gr|M|(CO)$_3$, that is isoelectronic to the sandwich structures of interest here. Although the aforementioned experimental works did not report the transport properties of the Bz|M|Gr complexes themselves, the reported loss of conductivity for the related structures is also consistent with the complex-formation at defect sites.

CONCLUSIONS

In summary, the defect-stabilized benzene-transition metal-graphene complexes offer an interesting route to functionalizing graphene while maintaining some of its

planar structure and hence, its high mobility. These complexes are interesting in their own right as they are prototypes of larger sandwich structures. For example, one can form sandwich structures by stacking layers of graphene sheets (or graphene and other low dimensional graphitic structures) with the transition metal atom(s) incorporated between them. In such complexes, the metal atoms may be used to dope the constituents, and/or to provide electrical tunneling between different layers [47]. Although predicted to form theoretically, it is hard to create these sandwich structures experimentally. Transition metals tend to cluster on pristine graphene due to their high mobilities on graphene and high elemental cohesivities. These issues can be remedied by deliberately engineering appropriate (acceptor-type) defects within the graphene web. The adatoms are shown to bind strongly to these sites. In this work we propose to use the latter to our advantage and create arrays of stable sandwich structures formed at the defect sites. Different defects within graphene lead to interesting variations in structural, electronic and magnetic properties of the intermediate transition metal-graphene complexes and the benzene-transition metal-graphene sandwich structures. These may prove advantageous for a number of applications in the fields of nano-electronics, spintronics and nano-magnetism.

[1] K. S. Novoselov, A. K. Geim, S. V. Morozov, D. Jiang, Y. Zhang, S. V. Dubonos, I. V. Grigorieva, and A. A. Firsov, Science **306**, 666 (2004), http://www.sciencemag.org/content/306/5696/666.full.pdf, URL http://www.sciencemag.org/content/306/5696/666.abstract.

[2] A. H. Castro Neto, F. Guinea, N. M. R. Peres, K. S. Novoselov, and A. K. Geim, Rev. Mod. Phys. **81**, 109 (2009), URL http://link.aps.org/doi/10.1103/RevModPhys.81.109.

[3] H. Terrones, R. Lv, M. Terrones, and M. S. Dresselhaus, Reports on Progress in Physics **75**, 062501 (2012), URL http://stacks.iop.org/0034-4885/75/i=6/a=062501.

[4] H. Pinto, R. Jones, J. P. Goss, and P. R. Briddon, Phys. Rev. B **82**, 125407 (2010), URL http://link.aps.org/doi/10.1103/PhysRevB.82.125407.

[5] S. M. Avdoshenko, I. N. Ioffe, G. Cuniberti, L. Dunsch, and A. A. Popov, ACS Nano **5**, 9939 (2011), http://pubs.acs.org/doi/pdf/10.1021/nn203719a, URL http://pubs.acs.org/doi/abs/10.1021/nn203719a.

[6] S. Sarkar, S. Niyogi, E. Bekyarova, and R. C. Haddon, Chem. Sci. **2**, 1326 (2011), URL http://dx.doi.org/10.1039/C0SC00634C.

[7] S. Sarkar, H. Zhang, J.-W. Huang, F. Wang, E. Bekyarova, C. N. Lau, and R. C. Haddon, Advanced Materials **25**, 1131 (2013), ISSN 1521-4095, URL http://dx.doi.org/10.1002/adma.201203161.

[8] P. Plachinda, D. R. Evans, and R. Solanki, The Journal of Chemical Physics **135**, 044103 (2011), URL http://scitation.aip.org/content/aip/journal/jcp/135/4/10.1063/1.3613649.

[9] Y.-H. Zhang, K.-G. Zhou, K.-F. Xie, H.-L. Zhang, Y. Peng, and C.-W. Wang, Phys. Chem. Chem. Phys. **14**, 11626 (2012), URL http://dx.doi.org/10.1039/C2CP41370A.

[10] V. M. Bermudez, *After many atempts, there was no equivocal evidence showing formation of bz—m—gr complexes.*, Personal Communication.

[11] V. M. Bermudez, Journal of Vacuum Science & Technology A: Vacuum, Surfaces, and Films **31**, 031402 (pages 8) (2013), URL http://link.aip.org/link/?JVA/31/031402/1.

[12] C. Kittel, *Introduction to Solid State Physics* (Wiley Eastern Limited, 1976), 5th ed.

[13] Q. Sun, Q. Wang, P. Jena, and Y. Kawazoe, Journal of the American Chemical Society **127**, 14582 (2005), http://pubs.acs.org/doi/pdf/10.1021/ja0550125, URL http://pubs.acs.org/doi/abs/10.1021/ja0550125.

[14] K. T. Chan, J. B. Neaton, and M. L. Cohen, Phys. Rev. B **77**, 235430 (2008), URL http://link.aps.org/doi/10.1103/PhysRevB.77.235430.

[15] G. Kim, S.-H. Jhi, N. Park, S. G. Louie, and M. L. Cohen, Phys. Rev. B **78**, 085408 (2008), URL http://link.aps.org/doi/10.1103/PhysRevB.78.085408.

[16] G. Kim, S.-H. Jhi, and N. Park, Applied Physics Letters **92**, 013106 (pages 3) (2008), URL http://link.aip.org/link/?APL/92/013106/1.

[17] S. Lee, M. Lee, and Y.-C. Chung, Journal of Applied Physics **113**, 17B503 (pages 3) (2013), URL http://link.aip.org/link/?JAP/113/17B503/1.

[18] D. Usachov, O. Vilkov, A. Grüneis, D. Haberer, A. Fedorov, V. K. Adamchuk, A. B. Preobrajenski, P. Dudin, A. Barinov, M. Oehzelt, et al., Nano Letters **11**, 5401 (2011), http://pubs.acs.org/doi/pdf/10.1021/nl2031037, URL http://pubs.acs.org/doi/abs/10.1021/nl2031037.

[19] J. P. Perdew and Y. Wang, Phys. Rev. B **33**, 8800 (1986).

[20] J. P. Perdew, K. Burke, and M. Ernzerhof, Phys. Rev. Lett. **77**, 3865 (1996).

[21] P. Giannozzi, S. Baroni, N. Bonini, M. Calandra, R. Car, C. Cavazzoni, D. Ceresoli, G. L. Chiarotti, M. Cococcioni, I. Dabo, et al., Journal of Physics: Condensed Matter **21**, 395502 (19pp) (2009), URL http://stacks.iop.org/0953-8984/21/i=39/a=395502.

[22] T. O. Wehling, A. I. Lichtenstein, and M. I. Katsnelson, Phys. Rev. B **84**, 235110 (2011), URL http://link.aps.org/doi/10.1103/PhysRevB.84.235110.

[23] V. I. Anisimov, F. Aryasetiawan, and A. I. Lichtenstein, J. Phys.: Condensed Matter **9**, 767 (1997), URL http://stacks.iop.org/0953-8984/9/i=4/a=002.

[24] D. Vanderbilt, Phys. Rev. B **41**, 7892 (1990).

[25] H. J. Monkhorst and J. D. Pack, Phys. Rev. B **13**, 5188 (1976).

[26] P. Dev, Y. Xue, and P. Zhang, Phys. Rev. Lett. **100**, 117204 (2008), URL http://link.aps.org/doi/10.1103/PhysRevLett.100.117204.

[27] P. Dev and P. Zhang, Phys. Rev. B **81**, 085207 (2010),

URL http://link.aps.org/doi/10.1103/PhysRevB.81.085207.

[28] P. Dev, H. Zeng, and P. Zhang, Phys. Rev. B **82**, 165319 (2010), URL http://link.aps.org/doi/10.1103/PhysRevB.82.165319.

[29] T. A. Abtew, Y. Y. Sun, B.-C. Shih, P. Dev, S. B. Zhang, and P. Zhang, Phys. Rev. Lett. **107**, 146403 (2011), URL http://link.aps.org/doi/10.1103/PhysRevLett.107.146403.

[30] J. G. Kushmerick, K. F. Kelly, H.-P. Rust, N. J. Halas, and P. S. Weiss, The Journal of Physical Chemistry B **103**, 1619 (1999), http://pubs.acs.org/doi/pdf/10.1021/jp983648v, URL http://pubs.acs.org/doi/abs/10.1021/jp983648v.

[31] A. Hashimoto, K. Suenaga, A. Gloter, K. Urita, and S. Iijima, Nature **430**, 870 (2004).

[32] C. P. Ewels, R. H. Telling, A. A. El-Barbary, M. I. Heggie, and P. R. Briddon, Phys. Rev. Lett. **91**, 025505 (2003), URL http://link.aps.org/doi/10.1103/PhysRevLett.91.025505.

[33] K. Nordlund, J. Keinonen, and T. Mattila, Phys. Rev. Lett. **77**, 699 (1996), URL http://link.aps.org/doi/10.1103/PhysRevLett.77.699.

[34] P. Esquinazi, D. Spemann, R. Höhne, A. Setzer, K.-H. Han, and T. Butz, Phys. Rev. Lett. **91**, 227201 (2003), URL http://link.aps.org/doi/10.1103/PhysRevLett.91.227201.

[35] A. W. Robertson, B. Montanari, K. He, C. S. Allen, Y. A. Wu, N. M. Harrison, A. I. Kirkland, and J. H. Warner, ACS Nano **7**, 4495 (2013), http://pubs.acs.org/doi/pdf/10.1021/nn401113r, URL http://pubs.acs.org/doi/abs/10.1021/nn401113r.

[36] B. R. K. Nanda, M. Sherafati, Z. S. Popovic̀, and S. Satpathy, New Journal of Physics **14**, 083004 (2012), URL http://stacks.iop.org/1367-2630/14/i=8/a=083004.

[37] T. Schiros, D. Nordlund, L. Pólová, D. Prezzi, L. Zhao, K. S. Kim, U. Wurstbauer, C. Gutiérrez, D. Delongchamp, C. Jaye, et al., Nano Letters **12**, 4025 (2012), http://pubs.acs.org/doi/pdf/10.1021/nl301409h, URL http://pubs.acs.org/doi/abs/10.1021/nl301409h.

[38] O. V. Yazyev, Reports on Progress in Physics **73**, 056501 (2010), URL http://stacks.iop.org/0034-4885/73/i=5/a=056501.

[39] S. Kattel, P. Atanassov, and B. Kiefer, The Journal of Physical Chemistry C **116**, 8161 (2012), http://pubs.acs.org/doi/pdf/10.1021/jp2121609, URL http://pubs.acs.org/doi/abs/10.1021/jp2121609.

[40] P. Dev and T. L. Reinecke, Phys. Rev. B **89**, 035404 (2014), URL http://link.aps.org/doi/10.1103/PhysRevB.89.035404.

[41] A. V. Krasheninnikov, P. O. Lehtinen, A. S. Foster, P. Pyykkö, and R. M. Nieminen, Phys. Rev. Lett. **102**, 126807 (2009), URL http://link.aps.org/doi/10.1103/PhysRevLett.102.126807.

[42] E. J. G. Santos, D. Sánchez-Portal, and A. Ayuela, Phys. Rev. B **81**, 125433 (2010), URL http://link.aps.org/doi/10.1103/PhysRevB.81.125433.

[43] B. Huang, J. Yu, and S.-H. Wei, Phys. Rev. B **84**, 075415 (2011), URL http://link.aps.org/doi/10.1103/PhysRevB.84.075415.

[44] S. di Vittorio, M. Dresselhaus, and G. Dresselhaus, Journal of Materials Research **8**, 1578 (1993), ISSN 2044-5326, URL http://journals.cambridge.org/article_S0884291400021075.

[45] I. Langmuir, Science **54**, 59 (1921), http://www.sciencemag.org/content/54/1386/59.full.pdf, URL `http://www.sciencemag.org/content/54/1386/59.short`.

[46] C. A. Tolman, Chem. Soc. Rev. **1**, 337 (1972), URL `http://dx.doi.org/10.1039/CS9720100337`.

[47] E. Y. Li and N. Marzari, ACS Nano **5**, 9726 (2011), http://pubs.acs.org/doi/pdf/10.1021/nn2032227, URL `http://pubs.acs.org/doi/abs/10.1021/nn2032227`.